Dynamic reanalysis of structures with geometric variability and parametric uncertainties via an adaptive model reduction method

J.-M. Mencik*,[a], N. Bouhaddi[b]

[a] *INSA Centre Val de Loire, Université d'Orléans, Université de Tours, Laboratoire de Mécanique Gabriel Lamé, Rue de la Chocolaterie, 41000 Blois, France*

[b] *Univ. Bourgogne Franche-Comté, FEMTO-ST Institute, CNRS/UFC/ENSMM/UTBM, Department of Applied Mechanics, 25000 Besançon, France*

Abstract

In this paper, a model reduction method is proposed for the dynamic reanalysis of structures with geometric variability and parametric uncertainties. Geometric variability is introduced by distorting the finite element meshes for some substructures via arbitrary shape functions. Parametric uncertainties are also considered to describe local variations of the stiffnesses of the substructures. The proposed approach involves expressing the substructure transformation matrices using interpolated matrices of Craig-Bampton component modes together with matrices of enrichment vectors. These enrichment vectors are parameter-independent and, as such, they only need to be computed once. This, as a result, leads to reduced substructure models which can be quickly updated to reanalyze structures with geometric and parametric changes. The accuracy and numerical efficiency of the proposed approach are highlighted through numerical experiments.

Key words: model reduction, finite element models, geometric variability, parametric uncertainties, matrix interpolation, subspace enrichment.

*Corresponding author

Email addresses: jean-mathieu.mencik@insa-cvl.fr (J.-M. Mencik), noureddine.bouhaddi@univ-fcomte.fr (N. Bouhaddi)

1. Introduction

The numerical prediction of the dynamic behavior of structures with geometric variability and parametric uncertainties is a problem of interest in mechanical engineering. This may concern, for instance, assemblies with several components which are connected via rubber blocks and springs as shown in Fig. 1, where the height of the rubber blocks is likely to vary in space (geometric variability) and where the stiffnesses of the springs could be random parameters (uncertainties). In practical situations, these structures are usually composed of substructures with different geometric changes, e.g., considering different kinds and levels of variability which can be introduced by considering distorted finite element (FE) meshes and shape functions – different between the substructures – as proposed in [1]. Also, parametric uncertainties can be introduced by considering random parameters that could represent some local variations of the stiffnesses of the substructures.

One of the major problems in structural dynamics concerns the computation of the eigenvalues and eigenvectors for some stiffness and mass matrices $\mathbf{K}$ and $\mathbf{M}$, and the computation of the related response functions. Accurate determination of these dynamic properties via finite elements usually involves considering many degrees of freedom (DOFs) which, despite the use of powerful processors, can make any dynamic analysis computationally cumbersome. Reducing the computational cost and, also, limiting the memory storage issues is becoming crucial, especially, in the design, optimization process and reliability analysis of structures. Model reduction methods represent good strategies to address these issues. Among these are:

(i) Subspace projection methods including modal truncation and Krylov-based techniques [2–4] where low-order modes and, eventually, high-order static correction terms are used.

(ii) Static condensation methods [5] or dynamic condensation methods where condensed mass and stiffness matrices, built from transformation matrices which can be frequency-dependent [6, 7]. Among these approaches is the Improved Reduced System (IRS) method [8] where an iterative procedure is proposed to compute the eigensolutions of structures. Many variants of this method consider an iterated improved reduced procedure and a substructuring scheme for undamped and non-classically damped structures [9–11]. These methods extend the condensation technique and provide an efficient solution for large-scale eigenvalue problems to compute eigensensitivities, structural responses and response sensitivities [12, 13]. On the other hand, reduction techniques for structures with frequency-dependent damping, such as structures treated with constrained viscoelastic layers, have been compared in [14] and extended to the aeroviscoelastic panel flutter

analysis in [15]. Also, the transient dynamic response of structural systems has been addressed in [16, 17] using time-domain condensation strategies that take into account linear and nonlinear viscoelastic systems, or multiple damping models.

(iii) Component Mode Synthesis (CMS) or substructuring methods where the reduced substructure matrices are built in an independent way and assembled to express the reduced model of a whole structure [18]. In this case, the reduced matrices of the substructures involve considering transformation matrices which are expressed from component modes. Among the substructuring techniques is the Craig-Bampton (CB) method [19] where the component modes of the substructures represent static/constraint modes and fixed interface modes. Substructuring techniques also include free interface methods [20, 21] and dual assembly approaches [22–25].

For substructures with varying FE meshes, varying properties or parametric uncertainties, substructuring techniques like the CB method raise, however, the issue of updating the transformation matrices as well as the reduced mass, damping and stiffness matrices many times, which may turn highly cumbersome. This especially concerns Monte Carlo simulations where many samples are usually required, e.g., to assess the sensitivity of the structure responses to several random parameters and several substructure meshes (geometric variability). In this case, several numerical tasks would need to be repeated many times for each modified substructure. This concerns: (i) the computation of the component (static and fixed interface) modes, (ii) the computation of the reduced mass, damping and stiffness matrices via matrix multiplications with the transformation matrix (Galerkin projection) and, also, (iii) the assembly of the reduced matrices of the new substructures.

CMS methods have been investigated in various ways in the literature to enhance the classical CB formulation [23, 26, 27]. Over the past two decades, fixed-interface CMS methods have been successfully improved by considering the high-order effects of the residual modes [26, 28–30]. The same principle can be adopted to improve free-interface CMS methods. However, the development of robust methods capable of modeling structures subject to mesh variations, structural changes or parametric uncertainties, without the need of updating the transformation matrices of the substructures many times, is not well reported. Some approaches based on Ritz-basis enrichment and combined approximations can be found in the literature, e.g., for the reanalysis of structures subject to structural changes [31–34], for the robust design of linear and nonlinear structures [35, 36] and for optimization problems [37]. The reanalysis of structures, for dynamic problems, turns highly complex and computationally cumbersome even for structures with moderate numbers of DOFs. Recent works have investigated the robustness of improved reduced models in presence of uncertainties [36, 38–42]. The objective of these methods is to fix the

computational burden associated with the increase of the number of random input parameters – i.e., the stochastic variability of a system – and the increase of the size of the numerical mechanical models which are used to describe the deterministic responses.

The main goal of the present study is to propose an improved substructuring technique which is accurate for the dynamic analysis of structures with mesh variations and parametric uncertainties such as localized stiffnesses. Considering both these geometric and parametric changes into a whole approach implying reduced models of substructures, easy to update to address these changes, does not seem to have been investigated so far. Specifically, a mixed modeling approach involving substructure transformation matrices built from interpolated component modes and enrichment vectors is proposed. The interpolated component modes are expressed via the strategy proposed in [1] and are used to describe the geometric changes of the substructures due to mesh variations. The enrichment vectors are issued from the static responses of the substructures due to parametric variations, and are here expressed in terms of parameter-independent vectors. The main advantages of the proposed substructure transformation matrices are: (i) they do not depend on the substructure parameters and (ii) they can be easily obtained by interpolation between a few interpolation points that concern some particular distorted meshes.

The rest of the paper is organized as follows. In Sec. 2, the FE modeling of structures involving several substructures with geometric variability and parametric uncertainties is addressed. The mixed modeling approach is detailed in Sec. 3. Especially, the substructure transformation matrices combining interpolated matrices of component modes and matrices of enrichment vectors are formulated in Sec. 3.4. Numerical experiments are carried out in Sec. 4. Two test cases are considered: (i) a 2D storey structure involving three parts with distorted FE meshes connected via rubber blocks and $2-$node spring elements with random stiffnesses; (ii) two Mindlin plates with localized random thickness and connected by springs with random stiffnesses, where the positions of the attachment points of the springs are subject to variability.

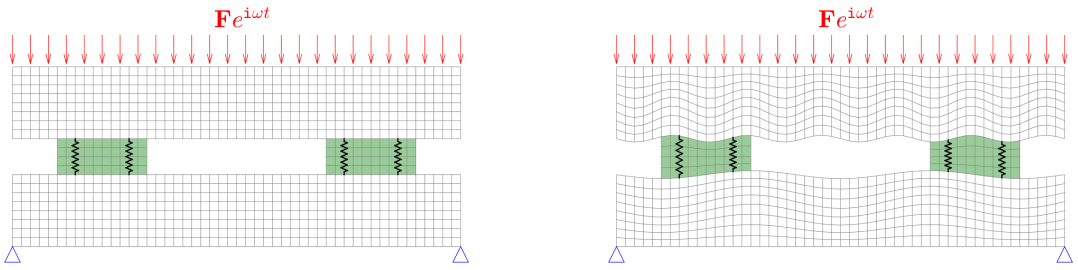

Figure 1: Arbitrary structure with two parts connected via rubber blocks (in green) and springs, which is subject to geometric variability and parametric uncertainties (springs). (left) FE mesh of the baseline structure; (right) distorted FE mesh.

2. Problem description

This paper concerns the dynamic analysis of linear elastic structures subject to geometric variability and parametric uncertainties, and undergoing harmonic disturbance with frequency $\omega/2\pi$. This could be, for instance, a 2D system in the (x, y) plane with two parts connected by means of rubber blocks and springs with random stiffnesses as shown in Fig. 1. Geometric variability is introduced here to describe, for instance, height imperfections at the interface between the two parts, hence impacting the dimensions of the rubber blocks as shown in Fig. 1. For practical purposes, a structure can be partitioned into several substructures whose variability can be governed in different ways. In some cases indeed, some substructures may undergo strong variability, the others being less (even not) impacted. Following the strategy proposed in [1], a substructure s ($s = 1, \ldots, n^s$) with geometric variability can be modeled by moving the positions of its nodes – i.e., (x^s_{j0}, y^s_{j0}) for some baseline FE mesh – using deterministic continuous "shape" functions $f^s_x(x, y)$ and $f^s_y(x, y)$ which are supposed to vanish at the interface with the other substructures to meet mesh compatibility conditions. In other words, geometric variability is taken into account by distorting the FE meshes of the baseline substructures. In this sense, the positions of the nodes of a substructure s are moved as follows:

$$x^s_j = x^s_{j0} + \epsilon^s_x f^s_x(x^s_{j0}, y^s_{j0}) \quad , \quad y^s_j = y^s_{j0} + \epsilon^s_y f^s_y(x^s_{j0}, y^s_{j0}), \tag{1}$$

where ϵ^s_x and ϵ^s_y are two real variables defined on $[-\delta^s\,,\,\delta^s]$ for some dispersion parameter δ^s. In the present framework, the shape functions $f^s_x(x, y)$ and $f^s_y(x, y)$ are supposed to be sufficiently smooth to prevent high element aspect ratios. Considering for instance Fig. 1, the structure can be partitioned into two substructures 1 and 2, with different mesh distortions, which are connected at the middle of the rubber blocks (central line where the positions of the nodes are kept constant) as shown in Fig. 2.

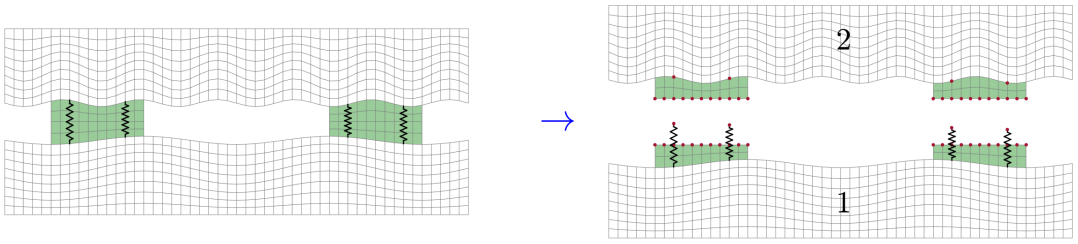

Figure 2: Structure partitioning via two substructures 1 and 2 with distorted FE meshes and parametric uncertainties (springs with random stiffnesses). Red dots highlight boundary DOFs.

Also assume that the substructures are subject to parametric uncertainties, e.g., considering vectors of random parameters $\mathbf{p}^s$ representing some local variations of the stiffnesses of the substructures. Hence,

the dynamic equilibrium equation of a substructure s may be written in the frequency domain as:

$$\left[-\omega^2\mathbf{M}^s(\mathbf{p}^s) + \mathtt{i}\omega\mathbf{C}^s(\mathbf{p}^s) + \mathbf{K}^s(\mathbf{p}^s)\right]\mathbf{u}^s = \mathbf{F}^s, \tag{2}$$

where $\mathbf{u}^s$ and $\mathbf{F}^s$ denote the displacement and force vectors (respectively), and $\mathbf{M}^s(\mathbf{p}^s)$, $\mathbf{C}^s(\mathbf{p}^s)$ and $\mathbf{K}^s(\mathbf{p}^s)$ denote the mass, damping and stiffness matrices (respectively) which result from distorting the FE mesh of the substructure, see Eq. (1). Note that, for stiffness-dependent damping, the matrix $\mathbf{C}^s$ is likely to be parameter-dependent. Also, the mass matrix $\mathbf{M}^s$ can be parameter-dependent too, e.g., considering stiffness variations which perturb the inertia of the substructure. The dynamic equation of a structure composed of several substructures follows as:

$$\left[-\omega^2\mathbf{M}(\mathbf{p}) + \mathtt{i}\omega\mathbf{C}(\mathbf{p}) + \mathbf{K}(\mathbf{p})\right]\mathbf{u} = \mathbf{F}, \tag{3}$$

where $\mathbf{M}(\mathbf{p})$, $\mathbf{C}(\mathbf{p})$ and $\mathbf{K}(\mathbf{p})$ are the mass, damping and stiffness matrices (respectively) which result from assembling the local matrices $\mathbf{M}^s(\mathbf{p}^s)$, $\mathbf{C}^s(\mathbf{p}^s)$ and $\mathbf{K}^s(\mathbf{p}^s)$ of the substructures; also, $\mathbf{p}$ denotes the whole vector of random parameters, defined by $\mathbf{p} = [(\mathbf{p}^1)^T\ (\mathbf{p}^2)^T\ \ldots\ (\mathbf{p}^{n^s})^T]^T$. The computation of the response functions of the structure – e.g., the displacement vector $\mathbf{u}$ measured at some points/nodes of a substructure – involves solving Eq. (3) many times for several discrete ~~pulsations~~ frequencies ω_i, e.g., $\omega_i = \omega_{min} + i(\omega_{max} - \omega_{min})/n_\omega$ for $i = 0, 1, \ldots, n_\omega$. To speed up this numerical task, reduced mass, damping and stiffness matrices are usually invoked. In dynamic substructuring, this means expressing the displacement vector $\mathbf{u}^s$ of the substructures – say, vectors of size $N^s \times 1$ – on the subspaces spanned by the column vectors of some transformation matrices $\widetilde{\mathbf{T}}^s$, of size $N^s \times M^s$ where $M^s \ll N^s$. In this framework, the displacement vectors of the substructures are approximated as $\mathbf{u}^s \approx \widetilde{\mathbf{T}}^s\widetilde{\mathbf{u}}^s$ with $\widetilde{\mathbf{u}}^s$ the reduced vectors (Galerkin projection of $\mathbf{u}^s$ onto the column space of $\widetilde{\mathbf{T}}^s$) which are obtained by solving the following global reduced matrix equation:

$$\left[-\omega^2\widetilde{\mathbf{M}}(\mathbf{p}) + \mathtt{i}\omega\widetilde{\mathbf{C}}(\mathbf{p}) + \widetilde{\mathbf{K}}(\mathbf{p})\right]\widetilde{\mathbf{u}} = \widetilde{\mathbf{F}}, \tag{4}$$

with

$$\widetilde{\mathbf{u}}^s = \mathcal{L}^s\widetilde{\mathbf{u}}, \tag{5}$$

where $\mathcal{L}^s$ are Boolean localization matrices for the substructures. In Eq. (4), $\widetilde{\mathbf{M}}(\mathbf{p})$, $\widetilde{\mathbf{C}}(\mathbf{p})$, $\widetilde{\mathbf{K}}(\mathbf{p})$ and $\widetilde{\mathbf{F}}$ are the reduced mass matrix, damping matrix, stiffness matrix and force vector of the structure which are built by assembling the local reduced matrices and vectors of the substructures. These are expressed by:

$$\widetilde{\mathbf{M}}^s(\mathbf{p}^s) = (\widetilde{\mathbf{T}}^s)^T\mathbf{M}^s(\mathbf{p}^s)\widetilde{\mathbf{T}}^s \quad , \quad \widetilde{\mathbf{C}}^s(\mathbf{p}^s) = (\widetilde{\mathbf{T}}^s)^T\mathbf{C}^s(\mathbf{p}^s)\widetilde{\mathbf{T}}^s \quad , \quad \widetilde{\mathbf{K}}^s(\mathbf{p}^s) = (\widetilde{\mathbf{T}}^s)^T\mathbf{K}^s(\mathbf{p}^s)\widetilde{\mathbf{T}}^s \tag{6}$$

and

$$\widetilde{\mathbf{F}}^s = (\widetilde{\mathbf{T}}^s)^T \mathbf{F}^s. \tag{7}$$

In the present case, however, a classical reduced modeling based on the transformation matrices $\widetilde{\mathbf{T}}^s$ of the substructures is prone to tough numerical issues. First notice that the same transformation matrices $\widetilde{\mathbf{T}}^s$ cannot be used to model substructures with varying FE meshes, which is the case when geometric variability is considered. This is explained because, since the mass, damping and stiffness matrices vary, the displacement vectors of the substructures need to be described in different subspaces. This means updating the transformation matrices of the substructures when variable FE meshes (mesh distortion) are considered, and therefore, computing the reduced mass, damping and stiffness matrices many times, see Eq. (6). As a second issue, parametric uncertainties involve, in addition, considering varying matrices $\mathbf{M}^s(\mathbf{p}^s)$, $\mathbf{C}^s(\mathbf{p}^s)$ and $\mathbf{K}^s(\mathbf{p}^s)$ of the substructures which also require the displacement vectors to be expressed in different subspaces. The development of a model reduction approach able to take into account both the geometric variability and parametric uncertainties of the substructures and perform low cost computation of the related reduced matrices in Eq. (6) is the main motivation behind the present paper. The key idea of the proposed strategy concerns the development of transformation matrices which can be quickly updated to address substructure changes, and which, as such, can be used efficiently for the reanalysis of structures. The methodology is detailed in the next section. The case of substructures with geometrical variability is considered first, see Sec. 3.2. The strategy to model substructures with parametric uncertainties is presented in Sec. 3.3. The mixed modeling approach for substructures with both geometric variability and parametric uncertainties is proposed in Sec. 3.4.

3. Adaptive model reduction

3.1. CB method

The proposed approach is based on the CB method whose main steps are recalled here for the sake of clarity. Thus, let us consider a structure which is composed of several substructures s ($s = 1, \ldots, n^s$) with mass, damping and stiffness matrices denoted by $\mathbf{M}^s$, $\mathbf{C}^s$ and $\mathbf{K}^s$, respectively. Also, let us partition the substructure meshes into boundary DOFs (B) encompassing the substructure interfaces/boundaries and the excitation points, and internal/other DOFs (I) which are supposed to be free from excitation. Hence, the dynamic equation of a substructure s can be written as follows:

$$\left[-\omega^2 \mathbf{M}^s + \mathrm{i}\omega \mathbf{C}^s + \mathbf{K}^s\right] \begin{bmatrix} \mathbf{u}^s_{\mathrm{B}} \\ \mathbf{u}^s_{\mathrm{I}} \end{bmatrix} = \begin{bmatrix} \mathbf{F}^s_{\mathrm{B}} \\ \mathbf{0} \end{bmatrix}, \tag{8}$$

where:

$$\mathbf{M}^s = \begin{bmatrix} \mathbf{M}^s_{\mathtt{BB}} & \mathbf{M}^s_{\mathtt{BI}} \\ \mathbf{M}^s_{\mathtt{IB}} & \mathbf{M}^s_{\mathtt{II}} \end{bmatrix} \quad , \quad \mathbf{C}^s = \begin{bmatrix} \mathbf{C}^s_{\mathtt{BB}} & \mathbf{C}^s_{\mathtt{BI}} \\ \mathbf{C}^s_{\mathtt{IB}} & \mathbf{C}^s_{\mathtt{II}} \end{bmatrix} \quad , \quad \mathbf{K}^s = \begin{bmatrix} \mathbf{K}^s_{\mathtt{BB}} & \mathbf{K}^s_{\mathtt{BI}} \\ \mathbf{K}^s_{\mathtt{IB}} & \mathbf{K}^s_{\mathtt{II}} \end{bmatrix}. \tag{9}$$

Also, denote by $N^s_{\mathtt{I}}$ and $N^s_{\mathtt{B}}$ the numbers of internal DOFs and boundary DOFs of a substructure s, respectively. Then, consider a reduced matrix of "fixed interface modes" $\widetilde{\mathbf{X}}^s = [\boldsymbol{\chi}^s_1 \cdots \boldsymbol{\chi}^s_{N^s_{\mathtt{CB}}}]$ where $\boldsymbol{\chi}^s_k$ ($k = 1, \ldots, N^s_{\mathtt{CB}}$) are the eigenvectors for the first $N^s_{\mathtt{CB}}$ (smallest) eigenvalues of the matrix pencil $(\mathbf{K}^s_{\mathtt{II}}, \mathbf{M}^s_{\mathtt{II}})$ with $N^s_{\mathtt{CB}} \ll N^s_{\mathtt{I}}$. Also, express the displacement vector $\mathbf{u}^s_{\mathtt{I}}$ in the subspace spanned by these $N^s_{\mathtt{CB}}$ fixed interface modes and the static modes – representing the column vectors of the matrix $-(\mathbf{K}^s_{\mathtt{II}})^{-1}\mathbf{K}^s_{\mathtt{IB}}$ – of the substructure. This yields $\mathbf{u}^s_{\mathtt{I}} \approx -(\mathbf{K}^s_{\mathtt{II}})^{-1}\mathbf{K}^s_{\mathtt{IB}}\widetilde{\mathbf{u}}^s_{\mathtt{B}} + \widetilde{\mathbf{X}}^s\widetilde{\boldsymbol{\alpha}}^s$, and therefore:

$$\begin{bmatrix} \mathbf{u}^s_{\mathtt{B}} \\ \mathbf{u}^s_{\mathtt{I}} \end{bmatrix} \approx \widetilde{\mathbf{T}}^s_{\mathtt{CB}} \begin{bmatrix} \widetilde{\mathbf{u}}^s_{\mathtt{B}} \\ \widetilde{\boldsymbol{\alpha}}^s \end{bmatrix} \quad \text{where} \quad \widetilde{\mathbf{T}}^s_{\mathtt{CB}} = \begin{bmatrix} \mathbf{I}_{N^s_{\mathtt{B}}} & \mathbf{0} \\ -(\mathbf{K}^s_{\mathtt{II}})^{-1}\mathbf{K}^s_{\mathtt{IB}} & \widetilde{\mathbf{X}}^s \end{bmatrix}. \tag{10}$$

Here, $\widetilde{\mathbf{T}}^s_{\mathtt{CB}}$ denotes the CB transformation matrix, $\widetilde{\mathbf{u}}^s_{\mathtt{B}}$ denotes an approximate of $\mathbf{u}^s_{\mathtt{B}}$ and $\widetilde{\boldsymbol{\alpha}}^s$ denotes a vector of generalized coordinates. Following the CB procedure, the dynamic equation of the substructure reduces to:

$$\left[-\omega^2\widetilde{\mathbf{M}}^s + \mathtt{i}\omega\widetilde{\mathbf{C}}^s + \widetilde{\mathbf{K}}^s\right] \begin{bmatrix} \widetilde{\mathbf{u}}^s_{\mathtt{B}} \\ \widetilde{\boldsymbol{\alpha}}^s \end{bmatrix} = \widetilde{\mathbf{F}}^s, \tag{11}$$

where $\widetilde{\mathbf{M}}^s$, $\widetilde{\mathbf{C}}^s$, and $\widetilde{\mathbf{K}}^s$ are the reduced mass, damping and stiffness matrices expressed by:

$$\widetilde{\mathbf{M}}^s = (\widetilde{\mathbf{T}}^s_{\mathtt{CB}})^T\mathbf{M}^s\widetilde{\mathbf{T}}^s_{\mathtt{CB}} \quad , \quad \widetilde{\mathbf{C}}^s = (\widetilde{\mathbf{T}}^s_{\mathtt{CB}})^T\mathbf{C}^s\widetilde{\mathbf{T}}^s_{\mathtt{CB}} \quad , \quad \widetilde{\mathbf{K}}^s = (\widetilde{\mathbf{T}}^s_{\mathtt{CB}})^T\mathbf{K}^s\widetilde{\mathbf{T}}^s_{\mathtt{CB}}. \tag{12}$$

Also, $\widetilde{\mathbf{F}}^s$ is the reduced force vector expressed by:

$$\widetilde{\mathbf{F}}^s = (\widetilde{\mathbf{T}}^s_{\mathtt{CB}})^T\mathbf{F}^s = \begin{bmatrix} \mathbf{F}^s_{\mathtt{B}} \\ \mathbf{0} \end{bmatrix}. \tag{13}$$

The modeling of a whole structure involving n^s substructures results from classical FE assembly procedure. This yields:

$$\left[-\omega^2\widetilde{\mathbf{M}} + \mathtt{i}\omega\widetilde{\mathbf{C}} + \widetilde{\mathbf{K}}\right] \begin{bmatrix} \widetilde{\mathbf{u}}_{\mathtt{B}} \\ \widetilde{\boldsymbol{\alpha}} \end{bmatrix} = \widetilde{\mathbf{F}}, \tag{14}$$

where

$$\begin{bmatrix} \widetilde{\mathbf{u}}^s_{\mathtt{B}} \\ \widetilde{\boldsymbol{\alpha}}^s \end{bmatrix} = \mathcal{L}^s \begin{bmatrix} \widetilde{\mathbf{u}}_{\mathtt{B}} \\ \widetilde{\boldsymbol{\alpha}} \end{bmatrix} \quad \text{for } s = 1, \ldots, n^s \qquad \text{where} \quad \widetilde{\boldsymbol{\alpha}} = \begin{bmatrix} \widetilde{\boldsymbol{\alpha}}^1 \\ \vdots \\ \widetilde{\boldsymbol{\alpha}}^{n^s} \end{bmatrix}, \tag{15}$$

with $\mathcal{L}^s$ the FE Boolean localization matrices of the substructures. Eq. (14) is a matrix equation of reduced size compared to Eq. (8) – which might be explained since the matrices of fixed interface modes $\widetilde{\mathbf{X}}^s$ of the substructures are of size $N^s_{\mathtt{I}} \times N^s_{\mathtt{CB}}$ with $N^s_{\mathtt{CB}} \ll N^s_{\mathtt{I}}$ – whose solutions are $\widetilde{\mathbf{u}}_{\mathtt{B}}$ and $\widetilde{\boldsymbol{\alpha}}$, and therefore $\widetilde{\mathbf{u}}^s_{\mathtt{B}}$ and $\widetilde{\boldsymbol{\alpha}}^s$, see Eq. (15). The displacement vectors of the substructures follows as $\mathbf{u}^s_{\mathtt{B}} \approx \widetilde{\mathbf{u}}^s_{\mathtt{B}}$ and $\mathbf{u}^s_{\mathtt{I}} \approx -(\mathbf{K}^s_{\mathtt{II}})^{-1}\mathbf{K}^s_{\mathtt{IB}}\widetilde{\mathbf{u}}^s_{\mathtt{B}} + \widetilde{\mathbf{X}}^s\widetilde{\boldsymbol{\alpha}}^s$.

3.2. Modeling by matrix interpolation: geometric variability

Consider now the case of substructures with varying geometric properties which are described via distorted FE meshes, see Fig. 2 for two substructures. The strategy for distorting the substructure FE meshes has been discussed earlier, see Eq. (1). It should be recalled that, for a given substructure s, f^s_x and f^s_y are two arbitrary functions of space (x, y) which vanish at the interface with the other substructures. Note that, if $f^s_x(x^s_{j0}, y^s_{j0}) = 0$ and $f^s_y(x^s_{j0}, y^s_{j0}) = 0$ for every node j, this means that the mesh of the substructure is undistorted (no variability). Also, if $f^s_x(x^s_{j0}, y^s_{j0}) \neq 0$ and $f^s_y(x^s_{j0}, y^s_{j0}) \neq 0$ for some node positions (x^s_{j0}, y^s_{j0}), and $f^s_x(x^s_{j0}, y^s_{j0}) = 0$ and $f^s_y(x^s_{j0}, y^s_{j0}) = 0$ elsewhere, then this means that the mesh distortion is localized to some subparts of the substructure.

Although well proven, the CB method (see Sec. 3.1) suffers from the fact that, in the present case, the transformation matrices $\widetilde{\mathbf{T}}^s_{\mathtt{CB}}$ of the substructures, Eq. (10), rely upon their mesh distortion which means that they need to be updated as soon as their geometric properties change. This makes any reanalysis (geometric variability) computationally cumbersome. To address this issue, it is proposed to approximate the transformation matrices $\widetilde{\mathbf{T}}^s_{\mathtt{CB}}$ by matrix interpolation. The procedure consists in computing the transformation matrices of the substructures for some points $((\epsilon^s_x)_p, (\epsilon^s_y)_p)$ (a small number) which refer to some particular distorted meshes, and estimating these matrices between these points by interpolation to analyze substructures with arbitrary mesh distortion parameters $(\epsilon^s_x, \epsilon^s_y)$. To interpolate the transformation matrices, they need to be expressed in compatible coordinate systems as discussed in [43]. For instance, an interpolation scheme based on eight interpolation points and eight Serendipity interpolation functions can be used, as proposed in [1]. This number of (eight) interpolation points seems to be a good compromise between the accuracy of the interpolation scheme and the computational load for expressing the transformation matrices at these points. The interpolation strategy in [1] also proposes to use Chebyshev points $\epsilon^s_x, \epsilon^s_y = \pm\delta^s/\sqrt{2}$ (δ^s being the mesh dispersion parameters introduced in Sec. 2) as interpolation points to better approximate the transformation matrices. The key steps of the procedure can be summarized as follows, for each substructure s ($s = 1, \ldots, n^s$):

1. Compute the matrix of static modes $-(\mathbf{K}^s_{\mathtt{II}})^{-1}\mathbf{K}^s_{\mathtt{IB}}$ and the reduced matrix of fixed interface modes $\widetilde{\mathbf{X}}^s$ at ~~Serendipity nodes~~ interpolation points $\left(\epsilon^s_x, \epsilon^s_y\right) = \left((\epsilon^s_x)_p, (\epsilon^s_y)_p\right)$ $(p = 1, \ldots, 8)$ with values $(\epsilon^s_x)_p$ and $(\epsilon^s_y)_p$ belonging to $\{-\delta^s/\sqrt{2}\,,\, 0\,,\, \delta^s/\sqrt{2}\}$ except $(\epsilon^s_x)_p = (\epsilon^s_y)_p = 0$:

$$-(\mathbf{K}^s_{\mathtt{II}})^{-1}_p(\mathbf{K}^s_{\mathtt{IB}})_p \quad \text{and} \quad \widetilde{\mathbf{X}}^s_p. \tag{16}$$

2. Introduce alternative matrices of fixed interface modes $\widehat{\mathbf{X}}^s_p$ to make them expressed in coordinate systems which are compatible (see [1, 43]):

$$\widehat{\mathbf{X}}^s_p = \widetilde{\mathbf{X}}^s_p \left((\mathbf{\Psi}^s)^T \widetilde{\mathbf{X}}^s_p\right)^{-1} \quad \text{where} \quad \mathbf{\Psi}^s = \left((\mathbf{M}^s_{\mathtt{II}})^{\frac{1}{2}}_0\right)^T \widetilde{\mathbf{X}}^s_0, \tag{17}$$

where notations $(\mathbf{M}^s_{\mathtt{II}})_0$ and $\widetilde{\mathbf{X}}^s_0$ mean that the matrices $\mathbf{M}^s_{\mathtt{II}}$ and $\widetilde{\mathbf{X}}^s$ are expressed for $\epsilon^s_x = 0$ and $\epsilon^s_y = 0$ (undistorted mesh).

3. Express the transformation matrix at interpolation points $\left((\epsilon^s_x)_p, (\epsilon^s_y)_p\right)$:

$$(\widehat{\mathbf{T}}^s_{\mathtt{CB}})_p = \begin{bmatrix} \mathbf{I}_{N^s_{\mathtt{B}}} & \mathbf{0} \\ -(\mathbf{K}^s_{\mathtt{II}})^{-1}_p(\mathbf{K}^s_{\mathtt{IB}})_p & \widehat{\mathbf{X}}^s_p \end{bmatrix}. \tag{18}$$

4. Interpolate the transformation matrix between interpolation points via Serendipity interpolation functions $N_p(\xi^s, \eta^s)$ [1]:

$$\widehat{\mathbf{T}}^s_{\mathtt{CB}} = \sum_{p=1}^{8} N_p(\xi^s, \eta^s)(\widehat{\mathbf{T}}^s_{\mathtt{CB}})_p = \sum_{p=1}^{8} N_p(\xi^s, \eta^s) \begin{bmatrix} \mathbf{I}_{N^s_{\mathtt{B}}} & \mathbf{0} \\ -(\mathbf{K}^s_{\mathtt{II}})^{-1}_p(\mathbf{K}^s_{\mathtt{IB}})_p & \widehat{\mathbf{X}}^s_p \end{bmatrix}, \tag{19}$$

where $\xi^s = (\sqrt{2}/\delta^s)\epsilon^s_x$ and $\eta^s = (\sqrt{2}/\delta^s)\epsilon^s_y$.

5. Approximate the reduced mass, damping and stiffness matrices, for any mesh parameters (ξ^s, η^s), as follows:

$$\widehat{\mathbf{M}}^s = (\widehat{\mathbf{T}}^s_{\mathtt{CB}})^T \mathbf{M}^s \widehat{\mathbf{T}}^s_{\mathtt{CB}} \quad , \quad \widehat{\mathbf{C}}^s = (\widehat{\mathbf{T}}^s_{\mathtt{CB}})^T \mathbf{C}^s \widehat{\mathbf{T}}^s_{\mathtt{CB}} \quad , \quad \widehat{\mathbf{K}}^s = (\widehat{\mathbf{T}}^s_{\mathtt{CB}})^T \mathbf{K}^s \widehat{\mathbf{T}}^s_{\mathtt{CB}}. \tag{20}$$

In this case, the reduced dynamic equations of the substructures write:

$$\left[-\omega^2 \widehat{\mathbf{M}}^s + \mathtt{i}\omega \widehat{\mathbf{C}}^s + \widehat{\mathbf{K}}^s\right] \begin{bmatrix} \widehat{\mathbf{u}}^s_{\mathtt{B}} \\ \widehat{\boldsymbol{\alpha}}^s \end{bmatrix} = \begin{bmatrix} \mathbf{F}^s_{\mathtt{B}} \\ \mathbf{0} \end{bmatrix}. \tag{21}$$

3.3. Modeling by subspace enrichment: parametric uncertainties

Reduced models of undistorted substructures with parameter-dependent mass, damping and stiffness matrices are investigated here. In this case, the dynamic equation of a substructure s writes:

$$\left[-\omega^2 \mathbf{M}_0^s(\mathbf{p}^s) + \mathtt{i}\omega \mathbf{C}_0^s(\mathbf{p}^s) + \mathbf{K}_0^s(\mathbf{p}^s)\right] \begin{bmatrix} \mathbf{u}_{\mathtt{B}}^s \\ \mathbf{u}_{\mathtt{I}}^s \end{bmatrix} = \begin{bmatrix} \mathbf{F}_{\mathtt{B}}^s \\ \mathbf{0} \end{bmatrix}, \tag{22}$$

where subscript 0 means that that the FE mesh of the substructure is undistorted. Also, $\mathbf{p}^s = [p_1^s\, p_2^s\, \ldots\, p_{n_p^s}^s]^T$ is a vector of uncertain parameters p_i^s which are here supposed to represent independent continuous random variables for some probability density functions $f_i^s(\mathscr{P}_i^s)$. Then, let us decompose the stiffness matrix of the substructure as follows:

$$\mathbf{K}_0^s(\mathbf{p}^s) = \underline{\mathbf{K}}_0^s + \Delta\mathbf{K}_0^s(\mathbf{p}^s), \tag{23}$$

where $\underline{\mathbf{K}}_0^s$ and $\Delta\mathbf{K}_0^s(\mathbf{p}^s)$ are, respectively, the mathematical expectation of $\mathbf{K}_0^s(\mathbf{p}^s)$ and the variation of the stiffness matrix due to parametric uncertainties:

$$\underline{\mathbf{K}}_0^s = \iint \cdots \int \mathbf{K}_0^s(\mathscr{P}_1^s, \ldots \mathscr{P}_{n_p^s}^s)\, f_1^s(\mathscr{P}_1^s) \ldots f_{n_p^s}^s(\mathscr{P}_{n_p^s}^s)\, d\mathscr{P}_1^s \ldots d\mathscr{P}_{n_p^s}^s, \tag{24}$$

and

$$\Delta\mathbf{K}_0^s(\mathbf{p}^s) = \mathbf{K}_0^s(\mathbf{p}^s) - \underline{\mathbf{K}}_0^s. \tag{25}$$

Again, a reduced modeling of the substructures can be considered. Following the idea proposed in [33], the displacement vector $\mathbf{u}_{\mathtt{I}}^s$ for the internal DOFs of a substructure s can be expressed in the subspace spanned by: (i) the static modes of the substructure with mean stiffness matrix $\underline{\mathbf{K}}_0^s$ (matrix $-(\underline{\mathbf{K}}_{\mathtt{II}}^s)_0^{-1}(\underline{\mathbf{K}}_{\mathtt{IB}}^s)_0$), (ii) the fixed interface modes of the substructure with mean stiffness matrix $\underline{\mathbf{K}}_0^s$, and mean mass matrix $\underline{\mathbf{M}}_0^s$, (matrix $\widetilde{\mathbf{X}}_0^s$) and (iii) enrichment vectors that represent the static responses of the mean substructure due to parametric variations. The enrichment basis represents the column vectors of $(\underline{\mathbf{K}}_{\mathtt{II}}^s)_0^{-1}\Delta\mathbf{F}_{\mathtt{I}}^s(\mathbf{p}^s)$ where $\Delta\mathbf{F}_{\mathtt{I}}^s(\mathbf{p}^s)$ is a matrix of residual (basis) force vectors resulting from parametric variations and which are induced here by the fixed interface modes of the mean substructure:

$$\Delta\mathbf{F}_{\mathtt{I}}^s(\mathbf{p}^s) = -\left[(\Delta\mathbf{K}_{\mathtt{II}}^s)_0(\mathbf{p}^s)\right]\widetilde{\mathbf{X}}_0^s. \tag{26}$$

Note that the column space of $\Delta\mathbf{F}_{\mathtt{I}}^s(\mathbf{p}^s)$ can be spanned by the column vectors of $-(\Delta\mathbf{K}_{\mathtt{II}}^s)_0\widetilde{\mathbf{X}}_0^s$ where $(\Delta\mathbf{K}_{\mathtt{II}}^s)_0$ represents $(\Delta\mathbf{K}_{\mathtt{II}}^s)_0(\mathbf{p}^s)$ for some particular values of parameters $\mathbf{p}^s$, e.g., the extreme ones [44]. In this way, a residual vector basis which does not depend on $\mathbf{p}^s$ can be proposed which, therefore,

only needs to be computed once. Hence, a suitable subspace for describing the parametric variations of the substructure can be defined as the column space of the following matrix:

$$\widetilde{\mathbf{T}}_{\mathtt{e}}^{s} = \begin{bmatrix} \mathbf{0} \\ \widetilde{\mathbf{X}}_{\mathtt{e}}^{s} \end{bmatrix}, \tag{27}$$

where $\widetilde{\mathbf{X}}_{\mathtt{e}}^{s}$ is the matrix of enrichment vectors ($N_{\mathtt{CB}}^{s}$ vectors) defined by:

$$\widetilde{\mathbf{X}}_{\mathtt{e}}^{s} = -(\underline{\mathbf{K}}_{\mathtt{II}}^{s})_0^{-1}(\Delta\mathbf{K}_{\mathtt{II}}^{s})_0\widetilde{\mathbf{X}}_{0}^{s}. \tag{28}$$

The enrichment vectors represent the static responses of the substructures to the residual forces, i.e., the column vectors of $\Delta\mathbf{F}_{\mathtt{I}}^{s} = -(\Delta\mathbf{K}_{\mathtt{II}}^{s})_0\widetilde{\mathbf{X}}_{0}^{s}$. For numerical conditioning purposes, it is advised to consider orthogonal enrichment vectors, and eventually a reduced number $N_{\mathtt{e}}^{s}$ of them where $N_{\mathtt{e}}^{s} \leq N_{\mathtt{CB}}^{s}$. In this sense, a "thin" singular value decomposition (SVD) of $\widetilde{\mathbf{X}}_{\mathtt{e}}^{s}$ can be invoked as:

$$\widetilde{\mathbf{X}}_{\mathtt{e}}^{s} = \mathbf{U}_{\mathtt{e}}^{s}\mathbf{\Sigma}_{\mathtt{e}}^{s}(\mathbf{V}_{\mathtt{e}}^{s})^{T}, \tag{29}$$

where $\mathbf{\Sigma}_{\mathtt{e}}^{s}$ denotes the $N_{\mathtt{CB}}^{s} \times N_{\mathtt{CB}}^{s}$ diagonal matrix of singular values (sorted in descending order) of $\widetilde{\mathbf{X}}_{\mathtt{e}}^{s}$, and $\mathbf{U}_{\mathtt{e}}^{s}$ and $\mathbf{V}_{\mathtt{e}}^{s}$ denote the related orthogonal matrices – i.e., $(\mathbf{U}_{\mathtt{e}}^{s})^{T}\mathbf{U}_{\mathtt{e}}^{s} = \mathbf{I}$ and $(\mathbf{V}_{\mathtt{e}}^{s})^{T}\mathbf{V}_{\mathtt{e}}^{s} = \mathbf{I}$ – of left singular vectors and right singular vectors, respectively. Especially, the column space of the matrix of left singular vectors $\mathbf{U}_{\mathtt{e}}^{s}$ is similar to that of $\widetilde{\mathbf{X}}_{\mathtt{e}}^{s}$, and as such, the column vectors of $\mathbf{U}_{\mathtt{e}}^{s}$ can be advantageously used as a reduced basis. In order to better regularize the projection/reduced basis, only a reduced set of singular vectors can be retained, i.e., those associated with the $N_{\mathtt{e}}^{s}$ highest singular values where $N_{\mathtt{e}}^{s} \leq N_{\mathtt{CB}}^{s}$. Hence, the following alternative reduced matrix can be proposed:

$$\widetilde{\mathbf{X}}_{\mathtt{e}}^{s} \rightarrow \widetilde{\mathbf{U}}_{\mathtt{e}}^{s} = \mathbf{U}_{\mathtt{e}}^{s}\left(:, 1{:}N_{\mathtt{e}}^{s}\right). \tag{30}$$

Eq. (30) means replacing $\widetilde{\mathbf{X}}_{\mathtt{e}}^{s}$ with the first $N_{\mathtt{e}}^{s}$ column vectors of $\mathbf{U}_{\mathtt{e}}^{s}$. As a result, the transformation matrices of the substructures become:

$$\widetilde{\mathbf{T}}_{0}^{s} = \left[\begin{array}{cc|c} \mathbf{I}_{N_{\mathtt{B}}^{s}} & \mathbf{0} & \mathbf{0} \\ -(\mathbf{K}_{\mathtt{II}}^{s})_0^{-1}(\mathbf{K}_{\mathtt{IB}}^{s})_0 & \widetilde{\mathbf{X}}_{0}^{s} & \widetilde{\mathbf{U}}_{\mathtt{e}}^{s} \end{array}\right]. \tag{31}$$

In this case, the displacement vectors (substructures) are approximated as follows:

$$\begin{bmatrix} \mathbf{u}_{\mathtt{B}}^{s} \\ \mathbf{u}_{\mathtt{I}}^{s} \end{bmatrix} \approx \widetilde{\mathbf{T}}_{0}^{s} \begin{bmatrix} \widetilde{\mathbf{u}}_{\mathtt{B}}^{s} \\ \widetilde{\boldsymbol{\beta}}_{0}^{s} \end{bmatrix}, \tag{32}$$

where $\widetilde{\boldsymbol{\beta}}_0^s$ are vectors of generalized coordinates. The reduced dynamic equations of the substructures follow as:

$$\left[-\omega^2\widetilde{\mathbf{M}}_0^s(\mathbf{p}^s)+\mathtt{i}\omega\widetilde{\mathbf{C}}_0^s(\mathbf{p}^s)+\widetilde{\mathbf{K}}_0^s(\mathbf{p}^s)\right]\begin{bmatrix}\widetilde{\mathbf{u}}_{\mathtt{B}}^s\\ \widetilde{\boldsymbol{\beta}}_0^s\end{bmatrix}=\begin{bmatrix}\mathbf{F}_{\mathtt{B}}^s\\ \mathbf{0}\end{bmatrix}, \tag{33}$$

where $\widetilde{\mathbf{M}}_0^s(\mathbf{p}^s)=(\widetilde{\mathbf{T}}_0^s)^T\mathbf{M}_0^s(\mathbf{p}^s)\widetilde{\mathbf{T}}_0^s$, $\widetilde{\mathbf{C}}_0^s(\mathbf{p}^s)=(\widetilde{\mathbf{T}}_0^s)^T\mathbf{C}_0^s(\mathbf{p}^s)\widetilde{\mathbf{T}}_0^s$ and $\widetilde{\mathbf{K}}_0^s(\mathbf{p}^s)=(\widetilde{\mathbf{T}}_0^s)^T\mathbf{K}_0^s(\mathbf{p}^s)\widetilde{\mathbf{T}}_0^s$.

3.4. Mixed modeling approach

Consider now substructures undergoing both geometric variability (mesh distortion) and parametric uncertainties, whose dynamic equations write:

$$\left[-\omega^2\mathbf{M}^s(\mathbf{p}^s)+\mathtt{i}\omega\mathbf{C}^s(\mathbf{p}^s)+\mathbf{K}^s(\mathbf{p}^s)\right]\begin{bmatrix}\mathbf{u}_{\mathtt{B}}^s\\ \mathbf{u}_{\mathtt{I}}^s\end{bmatrix}=\begin{bmatrix}\mathbf{F}_{\mathtt{B}}^s\\ \mathbf{0}\end{bmatrix}. \tag{34}$$

By combining the two previous approaches, the following transformation matrix, for each substructure s, can be proposed, see Eqs. (19) and (27):

$$\widehat{\mathbf{T}}^s=\sum_{p=1}^{8}N_p(\xi^s,\eta^s)\widehat{\mathbf{T}}_p^s, \tag{35}$$

where

$$\widehat{\mathbf{T}}_p^s=\left[\begin{array}{cc|c}\mathbf{I}_{N_{\mathtt{B}}^s} & \mathbf{0} & \mathbf{0}\\ -(\mathbf{K}_{\mathtt{II}}^s)_p^{-1}(\mathbf{K}_{\mathtt{IB}}^s)_p & \widehat{\mathbf{X}}_p^s & \widehat{\mathbf{U}}_{\mathtt{e}}^s\end{array}\right]. \tag{36}$$

Here, $\widehat{\mathbf{U}}_{\mathtt{e}}^s$ is the matrix of left singular vectors associated to the $N_{\mathtt{e}}^s$ highest singular values of the following matrix of enrichment vectors:

$$\widehat{\mathbf{X}}_{\mathtt{e}}^s=-(\underline{\mathbf{K}}_{\mathtt{II}}^s)_0^{-1}(\Delta\mathbf{K}_{\mathtt{II}}^s)_0\widehat{\mathbf{X}}_0^s, \tag{37}$$

where $\widehat{\mathbf{X}}_0^s=\widetilde{\mathbf{X}}_0^s((\boldsymbol{\Psi}^s)^T\widetilde{\mathbf{X}}_0^s)^{-1}$, see Eq. (17). The motivation behind considering $\widehat{\mathbf{X}}_0^s$ in Eq. (37), instead of $\widetilde{\mathbf{X}}_0^s$, is the use of compatible coordinate systems for reduced matrices of fixed interface modes, see Sec. 3.2. Also note that, to derive Eqs. (35) and (36), the well-known property that $\sum_{p=1}^{8}N_p(\xi^s,\eta^s)=1$ for Serendipity interpolation functions has been considered. In this case, the reduced dynamic equations of the substructures are given by:

$$\left[-\omega^2\widehat{\mathbf{M}}^s(\mathbf{p}^s)+\mathtt{i}\omega\widehat{\mathbf{C}}^s(\mathbf{p}^s)+\widehat{\mathbf{K}}^s(\mathbf{p}^s)\right]\begin{bmatrix}\widehat{\mathbf{u}}_{\mathtt{B}}^s\\ \widehat{\boldsymbol{\beta}}^s\end{bmatrix}=\begin{bmatrix}\mathbf{F}_{\mathtt{B}}^s\\ \mathbf{0}\end{bmatrix}, \tag{38}$$

where $\widehat{\mathbf{M}}^s(\mathbf{p}^s) = (\widehat{\mathbf{T}}^s)^T\mathbf{M}^s(\mathbf{p}^s)\widehat{\mathbf{T}}^s$, $\widehat{\mathbf{C}}^s(\mathbf{p}^s) = (\widehat{\mathbf{T}}^s)^T\mathbf{C}^s(\mathbf{p}^s)\widehat{\mathbf{T}}^s$ and $\widehat{\mathbf{K}}^s(\mathbf{p}^s) = (\widehat{\mathbf{T}}^s)^T\mathbf{K}^s(\mathbf{p}^s)\widehat{\mathbf{T}}^s$.

Remark. The proposed approach involves interpolating the transformation matrices $\widehat{\mathbf{T}}^s$ of the substructures (see Eq. (35)), instead of their reduced mass, damping and stiffness matrices [1]. Such a strategy is considered here to handle parametric uncertainties via interpolated transformation matrices based on enrichment vectors which are parameter-independent. This appears to be more relevant compared to when reduced matrices are interpolated. In this case indeed, this would mean performing interpolation on parametric spaces of high dimensions (depending on the number of uncertain parameters, in addition to mesh distortion), and therefore considering many interpolation points and excessive computations of the reduced matrices of the substructures at these interpolation points.

3.5. Discussion

The key idea behind the proposed approach is to consider transformation matrices $\widehat{\mathbf{T}}^s = \sum_{p=1}^{8} N_p(\xi^s, \eta^s)\widehat{\mathbf{T}}^s_p$ to express the reduced models of the substructures with geometric variability and parametric uncertainties, see Eqs. (35) and (36). The main advantage with these transformation matrices is that they can be quickly computed and updated to address changes into the substructure properties. In this framework indeed, this means computing, for each substructure, eight parameter-independent matrices $\widehat{\mathbf{T}}^s_p$ (once and for all), and expressing the transformation matrix $\widehat{\mathbf{T}}^s$ by interpolation which is very cheap from the computational point of view. In contrast, the classical CB method would require the transformation matrices of the substructures – implying their matrices of static modes and fixed interface modes – to be recomputed many times, which is a major problem when large-sized FE models are analyzed. More specifically, for each mesh and parameter change of a substructure, the classical CB method requires (see Sec. 3.1): (i) considering a matrix inverse and a matrix product for a $N^s_{\mathtt{I}} \times N^s_{\mathtt{I}}$ matrix $\mathbf{K}^s_{\mathtt{II}}$ to compute the matrix of static modes $-(\mathbf{K}^s_{\mathtt{II}})^{-1}\mathbf{K}^s_{\mathtt{IB}}$; (ii) solving via the Lanczos method an $N^s_{\mathtt{I}} \times N^s_{\mathtt{I}}$ eigenproblem for the matrix pencil $(\mathbf{K}^s_{\mathtt{II}}, \mathbf{M}^s_{\mathtt{II}})$ to obtain the reduced matrix of fixed interface modes $\widetilde{\mathbf{X}}^s$. Within the framework of the proposed approach, these tasks only need to be performed eight times, regardless of the substructure changes analyzed.

The second advantage of the proposed approach is in the computation of the reduced matrices $\widehat{\mathbf{M}}^s(\mathbf{p}^s)$, $\widehat{\mathbf{C}}^s(\mathbf{p}^s)$ and $\widehat{\mathbf{K}}^s(\mathbf{p}^s)$ in Eq. (38), which requires matrix products with $(\widehat{\mathbf{T}}^s)^T$ and $\widehat{\mathbf{T}}^s$. In fact, this numerical task can be strongly sped up for performing parametric analyses, e.g., Monte Carlo simulations for assessing the statistics of the dynamic responses of substructures of given mesh distortions subject to random parameters p^s_i. Indeed, it should be pointed out that the mass, damping and stiffness matri-

ces of the substructures are usually expressed as $\mathbf{M}^s(\mathbf{p}^s) = \underline{\mathbf{M}}^s + \Delta\mathbf{M}^s(\mathbf{p}^s)$, $\mathbf{C}^s(\mathbf{p}^s) = \underline{\mathbf{C}}^s + \Delta\mathbf{C}^s(\mathbf{p}^s)$ and $\mathbf{K}^s(\mathbf{p}^s) = \underline{\mathbf{K}}^s + \Delta\mathbf{K}^s(\mathbf{p}^s)$ where, in most situations, $\Delta\mathbf{M}^s(\mathbf{p}^s)$, $\Delta\mathbf{C}^s(\mathbf{p}^s)$ and $\Delta\mathbf{K}^s(\mathbf{p}^s)$ are strongly sparse matrices which, as such, can be quickly multiplied with $(\widehat{\mathbf{T}}^s)^T$ and $\widehat{\mathbf{T}}^s$. Other matrices $\underline{\mathbf{M}}^s$, $\underline{\mathbf{C}}^s$ and $\underline{\mathbf{K}}^s$ are parameter-independent, and in this sense, the matrix products associated with these matrices can be expressed as:

$$(\widehat{\mathbf{T}}^s)^T\underline{\mathbf{M}}^s\widehat{\mathbf{T}}^s = \sum_{q=1}^{8}\sum_{p=1}^{8} N_q(\xi^s,\eta^s)N_p(\xi^s,\eta^s)\left[(\widehat{\mathbf{T}}^s_q)^T\underline{\mathbf{M}}^s\widehat{\mathbf{T}}^s_p\right], \tag{39}$$

$$(\widehat{\mathbf{T}}^s)^T\underline{\mathbf{C}}^s\widehat{\mathbf{T}}^s = \sum_{q=1}^{8}\sum_{p=1}^{8} N_q(\xi^s,\eta^s)N_p(\xi^s,\eta^s)\left[(\widehat{\mathbf{T}}^s_q)^T\underline{\mathbf{C}}^s\widehat{\mathbf{T}}^s_p\right], \tag{40}$$

$$(\widehat{\mathbf{T}}^s)^T\underline{\mathbf{K}}^s\widehat{\mathbf{T}}^s = \sum_{q=1}^{8}\sum_{p=1}^{8} N_q(\xi^s,\eta^s)N_p(\xi^s,\eta^s)\left[(\widehat{\mathbf{T}}^s_q)^T\underline{\mathbf{K}}^s\widehat{\mathbf{T}}^s_p\right]. \tag{41}$$

In this case, each of the matrix products $(\widehat{\mathbf{T}}^s_q)^T\underline{\mathbf{M}}^s\widehat{\mathbf{T}}^s_p$, $(\widehat{\mathbf{T}}^s_q)^T\underline{\mathbf{C}}^s\widehat{\mathbf{T}}^s_p$ and $(\widehat{\mathbf{T}}^s_q)^T\underline{\mathbf{K}}^s\widehat{\mathbf{T}}^s_p$ needs to be computed 64 times, which could be achieved in a single pre-processing step regardless of the parametric changes. This appears to be an interesting feature of the proposed approach for performing Monte Carlo simulations where a large number (usually 1000 or more) of such matrix products would be required.

4. Numerical experiments

The relevance of the proposed approach is demonstrated considering two examples of moderate complexity. Sec. 4.1 focuses on the analysis of a 2D three storey structure with stiffened rubber blocks. Sec. 4.2 focuses on the analysis of two Mindlin plates connected by springs.

4.1. Three storey structure with stiffened rubber blocks

4.1.1. FE model

Let us consider a 2D storey structure involving three aluminum parts and four rubber blocks (in green), subjected to plane harmonic forces, as shown in Fig. 3. The material properties and nominal geometric properties (before mesh distortion) of the aluminum parts are similar and given by: Young's modulus of 70×10^9 Pa, density of 2700 kg/m^3, Poisson's ratio of 0.33, length of 1 m ($x-$direction), height of 0.1 m ($y-$direction) and thickness of 0.005 m. Also, the material properties and nominal geometric properties of the rubber blocks are given by (similar for all the blocks): Young's modulus of 150×10^6 Pa, density of 950 kg/m^3, Poisson's ratio of 0.48, length of 0.2 m ($x-$direction), height of 0.05 m ($y-$direction) and thickness of 0.005 m. The FE mesh of the structure is shown in Fig. 3 and involves 4-node plane stress quadrilateral elements. For each part/block, damping effects of Rayleigh

type are considered, i.e., considering a damping matrix of the form $\mathbf{C} = a\mathbf{M} + b\mathbf{K}$ with damping coefficients which are similar for all the parts. In addition to the rubber blocks, the aluminum parts are also connected via eight 2-node spring elements (black straight lines in Fig. 3) with 2 DOFs per node implying random stiffnesses along the $x-$ and $y-$directions with nominal values $k_x = 5 \times 10^7$ N/m and $k_y = 5 \times 10^5$ N/m. The whole structure is excited by two harmonic forces acting in opposite directions ($x-$axis) and is fixed at the bottom at $x = 0$ and $x = 1$ m as shown in Fig. 3. The harmonic response of the structure – i.e., the quadratic velocity $\omega^2|v|^2$ (v being the displacement along the $y-$ direction) at the top and middle of substructure 3 (Fig. 3) – is analyzed over a frequency band of $[0\,,\ 1500]$ Hz.

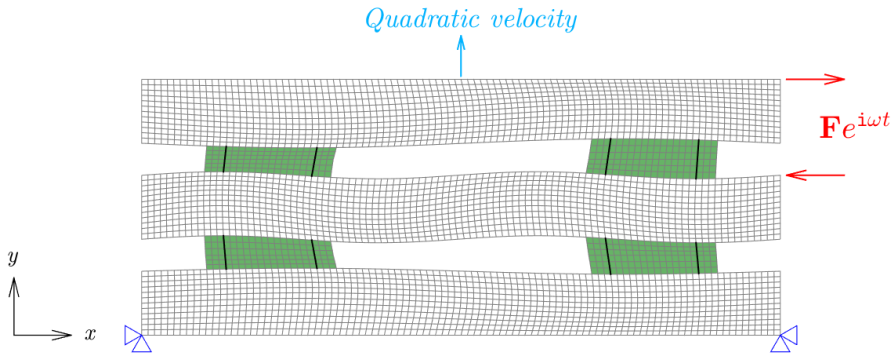

Figure 3: Three storey structure subject to geometric variability and involving 2-node spring elements (2 DOFs per node) with random stiffnesses (eight black straight lines). Rubber blocks are highlighted in green color.

4.1.2. Substructure model

It is proposed to partition the whole structure into three substructures 1, 2 and 3 as shown in Fig. 4. Geometric variability is introduced by distorting the FE meshes of the substructures via Eq. (1) where $f_x^s(x, y)$ and $f_y^s(x, y)$ are deterministic shape functions which can be chosen in a completely independent way between the substructures, e.g., to represent different kinds of geometric variability. For instance, in Figs. 3 and 4, $f_x^s(x, y)$ and $f_y^s(x, y)$ represent products of trigonometric functions of different periods, which are equal to zero at the interfaces between the substructures (central lines of the rubber blocks). Also, in Eq. (1), ϵ_x^s and ϵ_y^s denote mesh distortion parameters – different between the substructures – which quantify the levels/magnitudes of the geometric variability. Within the framework of the CB method, the substructures are modeled by means of static modes and fixed interface modes, as explained in Sec. 3.1. The related boundary nodes/DOFs are highlighted by red dots in Fig. 4. These represent the coupling DOFs, and also, the constraint DOFs (fixed nodes) and the excitation DOFs (substructures 2 and 3, $x-$direction only). Here, the numbers of fixed interface modes for modeling the substructures are $N_{\mathtt{CB}}^1 = 17$, $N_{\mathtt{CB}}^2 = 21$ and $N_{\mathtt{CB}}^3 = 18$. These numbers are supposed to be large enough and correspond

to the modes whose eigenfrequencies are below four times the maximum frequency of interest, i.e., 1500 Hz. In this way, the column spaces of the matrices of fixed interface modes of the substructures, and of the interpolated ones, are expected to be rich enough to accurately capture the dynamic behavior of the whole structure.

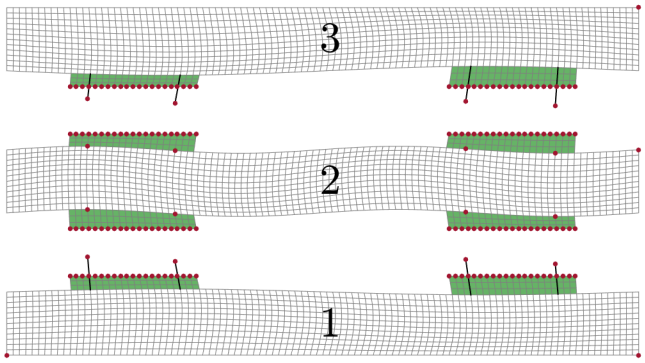

Figure 4: Substructures (three substructures 1, 2 and 3) involved in the modeling of the storey structure. Red dots highlight boundary DOFs (excitation points are described with one boundary DOF along the $x-$direction).

4.1.3. geometric variability

Geometric variability is introduced by distorting the FE meshes of the substructures from Eq. (1) with distortion parameters ϵ_x^s and ϵ_y^s defined on $[-\delta\,,\,\delta]$ where, in the present case, $\delta = 0.015$ m. Also, the shape functions $f_x^s(x,y)$ and $f_y^s(x,y)$ represent products of trigonometric functions (as explained earlier) and are such that $|f_x^s(x,y)| \leq 1$ and $|f_y^s(x,y)| \leq 1$. Such distorted FE meshes are shown in Fig. 5 together with the related frequency responses of the structure (quadratic velocity) for different values of ϵ_x^s and ϵ_y^s. The response functions issued from the interpolation strategy (Sec. 3.2) are plotted together with those issued from the full FE model of the structure (reference). Also, the response function of the baseline structure (without distortion) issued from the full FE model is plotted. It is first noticed that the response functions between each distorted structure and the baseline structure, and between two different distorted structures, can strongly differ, i.e., they are sensitive to geometric variability. On the other hand, for each case, it is shown that the proposed solution (interpolation) closely matches the reference one over the whole frequency band analyzed. This makes the interpolation strategy relevant for predicting the dynamic behavior of such structures.

In terms of computational loads, the reduced model (coupled substructures) involved in the interpolation strategy contains 242 DOFs. This includes the boundary DOFs (see Fig. 4, before substructure assembly) and the fixed interface modes of the substructures. In contrast, the full FE model of the struc-

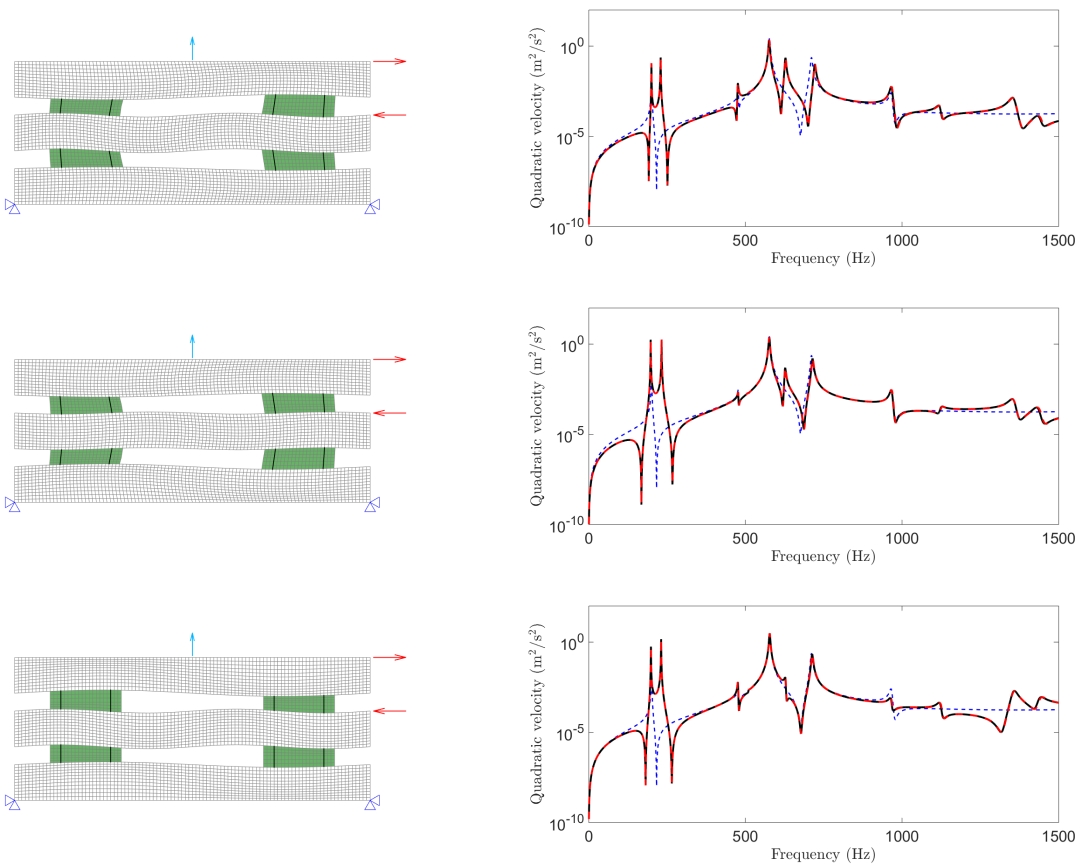

Figure 5: Some distorted FE meshes (left) and related frequency responses (right) of the storey structure: (black continuous line) reference; (red dashed line) interpolation; (blue dashed line) baseline structure (undistorted mesh).

ture contains 8714 DOFs. The related time reduction to solve the dynamic equation of the structure – i.e., the reduced equation obtained by assembling the substructure models (21), vs Eq. (3) – is roughly $90 - 95\%$ to the benefit of the proposed approach.

To further demonstrate the relevance and accuracy of the interpolation strategy, an extreme case involving substructures with mesh distortion parameters $(\epsilon_x^s, \epsilon_y^s)$ far from the interpolation points is considered. The chosen parameters are $(\epsilon_x^1, \epsilon_y^1) = (-\delta, \delta)$, $(\epsilon_x^2, \epsilon_y^2) = (\delta, \delta/2\sqrt{2})$ and $(\epsilon_x^3, \epsilon_y^3) = (-\delta, -\delta)$ where it is recalled that the interpolation points correspond to $(\epsilon_x^s)_p, (\epsilon_y^s)_p \in \{-\delta/\sqrt{2}\,,\, 0\,,\, \delta/\sqrt{2}\}$. The related distorted meshes of the substructures and frequency responses are shown in Fig. 6 with a focus on the frequency band $[450\,,\, 850]$ Hz highlighting a few resonance peaks which are sensitive to geometric changes. In this case again, the proposed approach shows good agreement with the FE solutions.

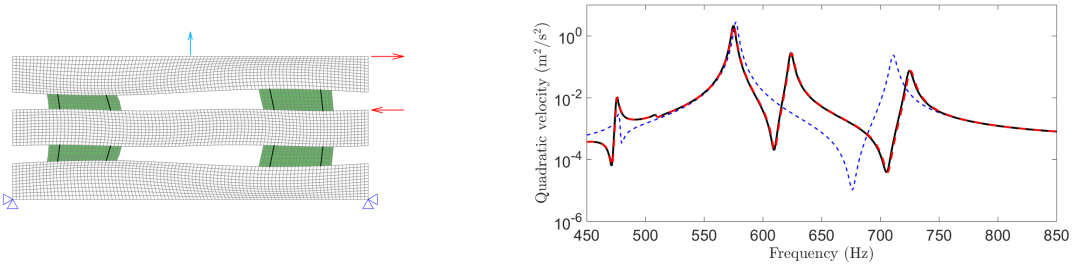

Figure 6: Substructures with mesh distortion parameters $(\epsilon_x^1, \epsilon_y^1) = (-\delta, \delta)$, $(\epsilon_x^2, \epsilon_y^2) = (\delta, \delta/2\sqrt{2})$ and $(\epsilon_x^3, \epsilon_y^3) = (-\delta, -\delta)$ (left) and related frequency responses on $[450\,,\,850]$ Hz (right): (black continuous line) reference; (red dashed line) interpolation; (blue dashed line) baseline structure (undistorted mesh).

4.1.4. geometric variability and parametric uncertainties

Consider now the case where the structure undergoes both geometric variability (mesh distortion) and parametric uncertainties. Here, the stiffnesses of the spring elements in Fig. 3 represent 16 random independent variables which are supposed to follow a uniform distribution on $[0\,,\,10^8]$ N/m for k_x, and $[0\,,\,10^6]$ N/m for k_y. Regarding the dynamic equation in Eq. (2), these random stiffnesses are introduced by means of two 8×1 vectors of parameters $\mathbf{p}^1$ and $\mathbf{p}^3$ for modeling substructures 1 and 3, respectively. The response function of the structure (full FE model) for a given set of mesh distortion parameters ϵ_x^s and ϵ_y^s and a given set of random parameters $\mathbf{p}^1$ and $\mathbf{p}^3$ is shown in Fig. 7 (black curve). For the sake of clarity, the response function of the distorted structure with nominal stiffnesses $k_x = 5 \times 10^7$ N/m and $k_y = 5 \times 10^5$ N/m is not shown (the reader is referred to Fig. 5, top figure). It is, however, dissimilar from the curve shown in Fig. 7.

First, the interpolation strategy proposed in Sec. 3.2 is considered, as earlier. The related response function is shown in Fig. 7 (left figure), and in this case, it shows strong dissimilarities with the reference curve. The differences between the proposed and reference solutions clearly appear after 700 Hz, but also at lower frequencies at the resonance peaks of the structure (frequency shifts). This lack of accuracy might be explained since the subspaces spanned by the interpolated static modes and fixed interface modes of the substructures are not rich enough to take into account the stiffness variations of the spring elements. Besides, it should be pointed out that, contrary to what could be expected, increasing the number of fixed interface modes for modeling the substructures deteriorates the convergence of the strategy. The issue is linked to finding, within the framework of the interpolation strategy, a common subspace for matrices of modes which, for part of them – say, those associated to very large eigenfrequencies —, are spurious since quite disconnected from the other ones.

On the other hand, the response function issued from the mixed modeling approach proposed in

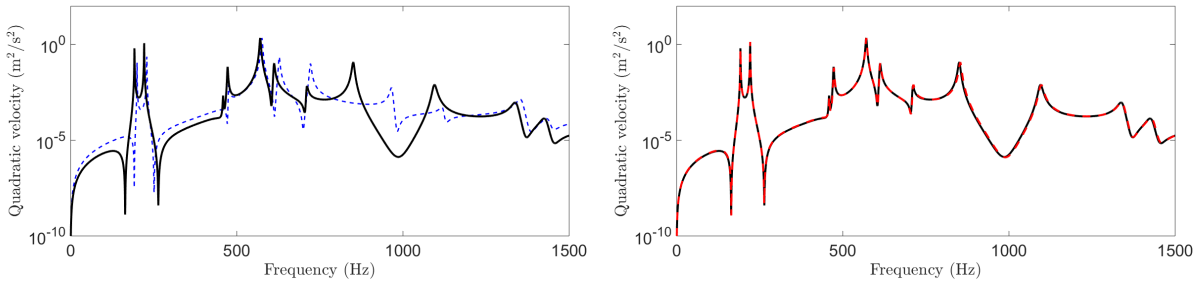

Figure 7: Frequency response of the storey structure with both geometric variability and parametric uncertainties (one set of parameters): (black continuous line) reference; (left, blue dashed line) interpolation; (right, red dashed line) interpolation with enrichment.

Sec. 3.4, which combines both interpolated matrices of component modes and matrices of enrichment vectors, can be computed as shown in Fig. 7 (right figure). Here, $N_{\mathtt{e}}^1 = N_{\mathtt{CB}}^1 = 17$ and $N_{\mathtt{e}}^3 = N_{\mathtt{CB}}^3 = 18$ enrichment vectors are considered for modeling substructures 1 and 3, in addition to the interpolated ones. As for substructure 2, it is modeled using interpolated modes only (no spring element). In this case, the proposed solution correctly agrees with the reference one, as expected. This, therefore, highlights the need of using the mixed modeling approach for structures with both geometric variability and parametric variations.

From the computational point of view, the sizes of the reduced matrices remain small compared to the reference model, i.e., 277 DOFs for the reduced dynamic equation of the structure, against 242 DOFs with the sole interpolation strategy. The related time reduction, to solve the dynamic equation of the structure, is almost similar to the previous case ($90 - 95\%$). It should be recalled that, within the framework of the proposed approach, several low-cost "offline" numerical tasks are required. These concern (i) the computation of the transformation matrices $\widehat{\mathbf{T}}^s$ of the substructures and (ii) the computation of the reduced matrices of the substructures via matrix products with $(\widehat{\mathbf{T}}^s)^T$ and $\widehat{\mathbf{T}}^s$. These numerical tasks can be strongly sped up as explained in Sec. 3.5. The related computational times are here negligible compared to the cost for computing the response function.

4.1.5. Monte Carlo analysis

The proposed approach (Sec. 3.4), while providing low computational times, has proven relevant for predicting the dynamic behavior of the structure with both geometric variability and parametric uncertainties. As such, it can be advantageously used for a Monte Carlo analysis, e.g., considering $N_{\mathtt{MC}} = 1000$ samples of random stiffnesses (2×8 values for k_x and k_y) which can be obtained via any Latin Hypercube sampling method – e.g., the one provided by the MATLAB's function lhfdesign. For instance, the

confidence interval about the mean value of the measured quadratic velocity may be predicted. For a confidence level of 95%, it is given by:

$$I = \left[\bar{X} - 1.96\sqrt{\frac{S}{N_{\texttt{MC}}}} \ , \ \bar{X} + 1.96\sqrt{\frac{S}{N_{\texttt{MC}}}} \right], \tag{42}$$

where $\bar{X}$ and S are estimates of the mean and variance of the quadratic velocity which can be iteratively computed from the strategy proposed in [45]. The mean of the quadratic velocity and the related confidence interval are shown in Fig. 8 on the frequency band $[700\,,\,1500]$ Hz. It is shown that the structure response is highly sensitive to uncertainties on $[800\,,\,1100]$ Hz, which is somewhat in accordance with the response function in Fig. 7. In this frequency band, the average relative error for predicting the mean value – say, $2 \times (1.96\sqrt{S/N_{\texttt{MC}}})/\bar{X}$ – is about $30 - 40\%$.

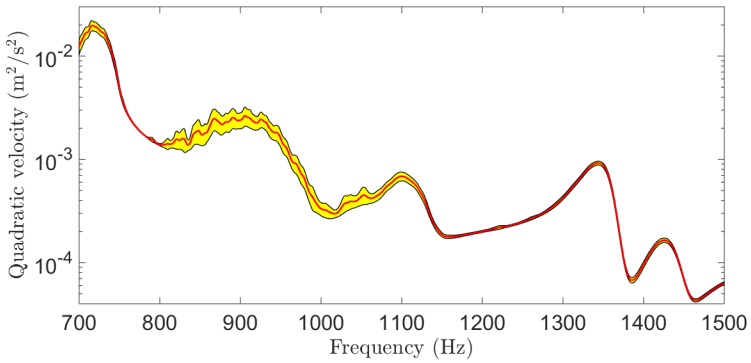

Figure 8: Mean of the measured quadratic velocity (red line) and related confidence interval (yellow area).

4.2. Two coupled plates

4.2.1. FE model

Consider now the case of two square Mindlin plates 1 and 2, clamped on one of their edges, which are connected together via an array of 9×3 springs whose attachment positions on plate 1 are subject to variations as shown in Fig. 9 where FE mesh distortion is highlighted in blue area. Parametric uncertainties are introduced here considering random stiffnesses for the springs and, also, a square central part of plate 2 with random thickness h (see red area in Fig. 9). In addition, plate 2 is excited at its center by a transverse harmonic force, i.e., at the center of the "uncertain" region highlighted in red in Fig. 9. Both plates share similar nominal characteristics, i.e.: Young's modulus of 210×10^9 Pa, density of 7800 kg/m^3, Poisson's ratio of 0.33, dimensions of 1×1 m^2 and thickness of 0.002 m. Also, the dimensions of the red central part of plate 2 is 0.25×0.25 m^2. The FE meshes of the plates are shown in Fig. 9 and involve 4-node Mindlin plate elements (40×40 elements for each plate) with 3 DOFs per node [46].

To overcome shear locking effects, the "shearing part"of the stiffness matrices of the plate elements is computed using a reduced number of Gauss points (one point here), which is standard. Again, damping of Rayleigh type is considered for modeling the plates (same damping coefficients). As for the springs, they share the same nominal stiffness $k = 5 \times 10^4$ N/m. In the present case, the averaged value of the quadratic velocities (transverse direction) for the nodes in plate 1 which do not belong to the distorted part – i.e., all the nodes except those contained in the blue area – is assessed. The related frequency response is analyzed over a frequency band of $[0\,,\,100]$ Hz.

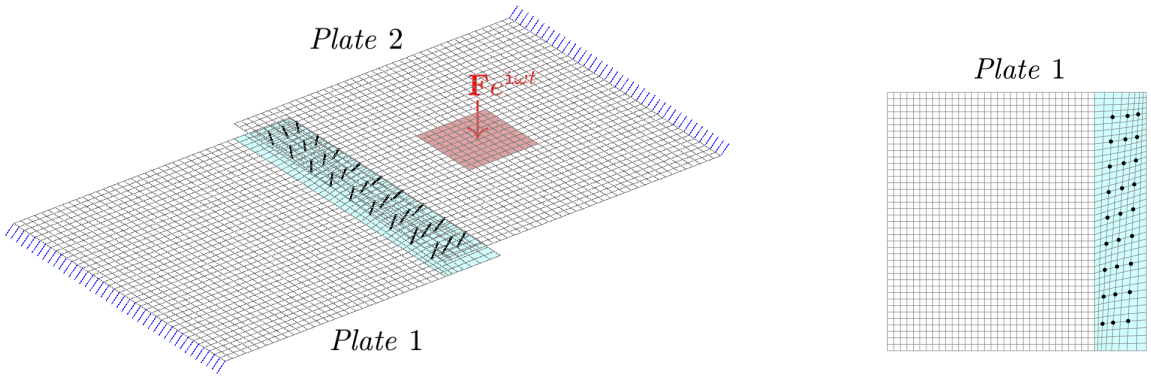

Figure 9: (left) Two coupled plates with geometric variability, springs with random stiffnesses (black straight lines), and localized random thickness (red patch). (right) Distorted FE mesh of plate 1. Distorted FE mesh only concerns plate 1 (blue area).

4.2.2. Substructure model

The whole structure can be straightforwardly partitioned into two substructures 1 and 2 as shown in Fig. 10 which represent, respectively, plate 1 (including part with distorted FE mesh) with the springs, and plate 2 (including central part with random thickness). The distortion of the FE mesh of plate 1 is obtained by moving the positions of its nodes via Eq. (1) where $f_x^s(x,y) = f_x^1(x,y)$ and $f_y^s(x,y) = f_y^1(x,y)$ are null except on the blue part (see Fig. 9). In this case, $f_x^1(x,y)$ and $f_y^1(x,y)$ represent products of trigonometric and polynomial functions which are such that $f_x^1(x,y) = 0$ on the main two edges of the blue part, and $f_y^1(x,y) = 0$ on the other two edges. A schematic of such a distorted FE mesh is shown in Fig. 9. The boundary nodes/DOFs of the substructures are highlighted by red dots in Fig. 10 and include the coupling DOFs between the springs and plate 2, the constraint DOFs (fixed nodes) and the excitation DOF (substructure 2). Here, the numbers of fixed interface modes for modeling substructures 1 and 2 are $N_{\mathtt{CB}}^1 = 83$ and $N_{\mathtt{CB}}^2 = 68$, respectively. These numbers are supposed to be large enough and correspond to the modes whose eigenfrequencies are below five times the maximum frequency of interest

(100 Hz). A good strategy to determine these numbers of modes is to perform a sensitivity analysis, i.e., by investigating the accuracy of the response function for different numbers of modes.

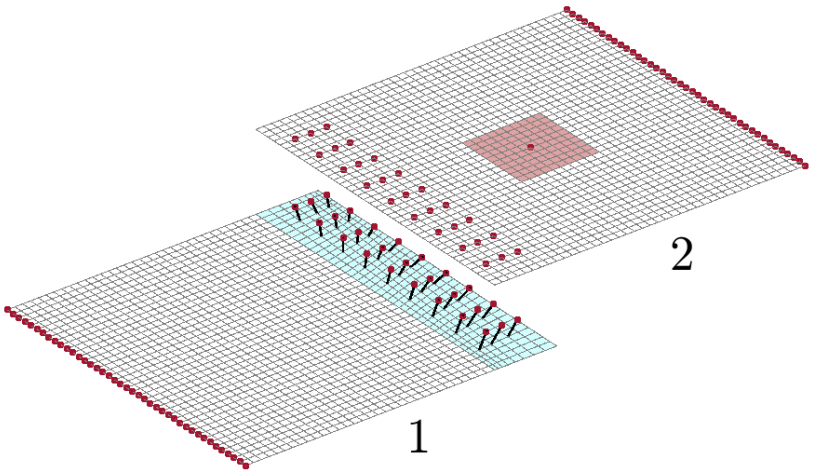

Figure 10: Substructures representing one plate with distorted FE mesh and springs with random stiffnesses (substructure 1), and one plate with localized random thickness (substructure 2). Red dots highlight boundary DOFs (excitation point is described with one boundary DOF along the transverse direction).

4.2.3. geometric variability and parametric uncertainties: springs with random stiffnesses

Geometric variability is introduced by distorting the FE mesh of plate 1 via Eq. (1), where $f_x^s(x,y) = f_x^1(x,y)$ and $f_y^s(x,y) = f_y^1(x,y)$ are such that $|f_x^1(x,y)| \leq 1$ and $|f_y^1(x,y)| \leq 2$ on the blue part in Fig. 9, and $f_x^1(x,y) = 0$ and $f_y^1(x,y) = 0$ elsewhere. Here, the mesh distortion parameters – i.e., $\epsilon_x^s = \epsilon_x^1$ and $\epsilon_y^s = \epsilon_y^1$, see Eq. (1) – are defined on $[-\delta^1\,,\,\delta^1]$ where $\delta^1 = 0.035$ m. On the other hand, the stiffnesses of the springs are supposed to represent 27 independent random variables following a uniform distribution on $[0\,,\,10^5]$ N/m. The response function (averaged quadratic velocity, plate 1) of the structure, for a given set of mesh distortion parameters ϵ_x^1 and ϵ_y^1 and a given set of random stiffnesses (27 different parameters) is shown in Fig. 11. The mesh distortion considered here is similar to that shown in Fig. 9. The solution issued from the full FE model of the structure is shown together with that provided by the mixed modeling approach proposed in Sec. 3.4. Within the framework of the proposed approach, $N_{\mathsf{e}}^1 = N_{\mathsf{CB}}^1 = 83$ enrichment vectors are considered for modeling substructure 1, in addition to the interpolated component modes. The related reduced model of the whole structure involves 262 DOFs (including boundary DOFs, fixed interface modes of the substructures, enrichment vectors for substructure 1), against 9840 DOFs for the full FE model. To highlight the influence of the random stiffnesses, the response function of the distorted structure with nominal stiffnesses $k = 5 \times 10^4$ N/m is

also shown in Fig. 11 (see blue dashed line). Here, the response functions of the structure cover many resonance peaks involving the global resonance modes of the structure, and also, the local resonance ones of the plates. Overall this yields a non-smooth frequency spectrum with non-uniform modal density and resonance peaks of different magnitudes. Again, the proposed approach appears relevant for predicting the dynamic behavior of the structure, i.e., the related response function closely matches the reference solution over the whole frequency range analyzed. The main interest of the proposed approach lies in the reduction of the computational times, i.e., more than 95% (compared to computing the full FE model) in the present case.

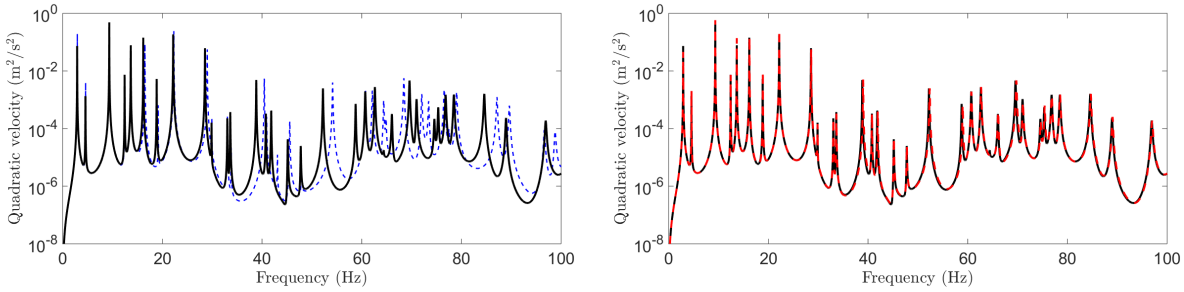

Figure 11: Frequency response of the coupled plates with geometric variability and parametric uncertainties which concern springs with random stiffnesses (one set of parameters): (black continuous line) reference; (left, blue dashed line) structure with nominal stiffnesses; (right, red dashed line) interpolation with enrichment.

4.2.4. *geometric variability and parametric uncertainties: springs with random stiffnesses and localized random thickness in plate* 2

Let us consider, finally, the same structure as before with an additional random parameter which concerns the thickness h of the red square part (plate 2) shown in Fig. 9, which is supposed to randomly vary on 0.002 m $\pm\, 30\%$ with a uniform probability law. Again, the mixed modeling approach proposed in Sec. 3.4 is investigated. Here, $N_{\mathtt{e}}^1 = N_{\mathtt{CB}}^1 = 83$ enrichment vectors are considered for modeling substructure 1 (as before), and $N_{\mathtt{e}}^2 = 30$ enrichment vectors are considered for modeling substructure 2. This yields a reduced model with 292 DOFs (including boundary DOFs, fixed interface modes of the substructures, enrichment vectors for substructures 1 and 2). The added enrichment vectors, for substructure 2, are computed from Eq. (28) where $(\Delta\mathbf{K}^s_{\mathtt{II}})_0 = (\Delta\mathbf{K}^2_{\mathtt{II}})_0$ represents the variation of the stiffness matrix of substructure 2 resulting from the variation of the thickness of the central part. Note that, although not negligible, the variation of the mass matrix of the substructure (thickness variation) is not taken into account in the expression of the enrichment vectors. In other words, only the static contribution of the variation of the dynamic stiffness matrix of the structure is considered to express the

enrichment vectors. The related response function is shown in Fig. 12 together with the reference FE solution. Again, a given set of random parameters is considered (same stiffnesses as in the last subsection, and a given value of h). To highlight the influence of the random thickness, the response function of the structure with nominal thickness $h = 0.002$ m is also shown in Fig. 12 in blue dashed line. In this case again, the proposed approach successfully predicts the dynamic response of the structure without any ambiguity. As for the previous case, the reduction of the computational times appear to be greater than 95%.

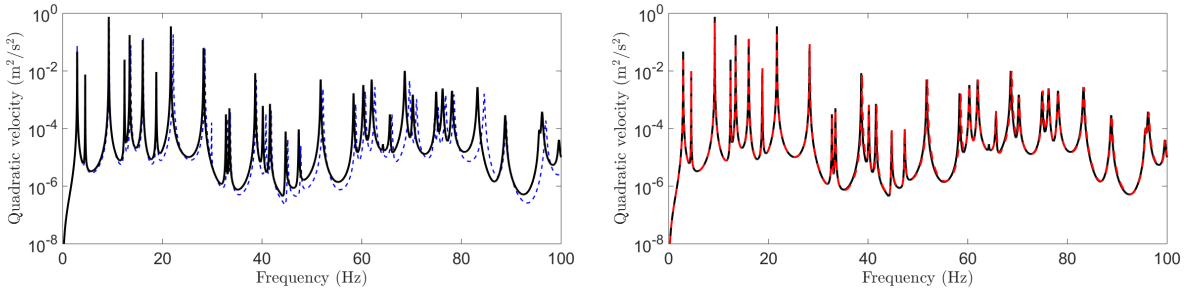

Figure 12: Frequency response of the coupled plates with geometric variability and parametric uncertainties which concern springs with random stiffnesses and localized random thickness (one set of parameters): (black continuous line) reference; (left, blue dashed line) structure with random stiffnesses and nominal thickness; (right, red dashed line) interpolation with enrichment.

5. Conclusion

A model reduction method has been proposed for the reanalysis of structures composed of substructures with geometric variability and parametric uncertainties. Geometric variability is introduced by distorting the FE meshes of the substructures via shape functions. On the other hand, parametric uncertainties are introduced to describe local variations of the stiffness matrices of the substructures. The proposed approach involves considering substructure transformation matrices, easy to update to address such substructure changes, which are built from interpolated matrices of component modes and matrices of enrichment vectors. In this framework, the transformation matrices can be estimated by interpolation between "interpolation points" $\widehat{\mathbf{T}}_p^s$ which represent parameter-independent matrices which only need to be computed once (i.e., regardless of the substructure changes). This strategy leads the way to computing the reduced matrices of the substructures efficiently without the need of performing matrix products between the mass/damping/stiffness matrices and the transformation matrices many times, which is of main concern for Monte Carlo simulations. Numerical experiments have been carried out considering two structures of moderate complexity, i.e., a 2D storey structure with stiffened rubber blocks and two

Mindlin plates connected by springs. In the first case, parametric uncertainties have been introduced via spring elements of random stiffnesses. As for the second one, they have been introduced via springs of random stiffnesses, and random thickness localized somewhere on a plate. For these cases, the proposed approach has proven accurate for predicting the harmonic responses of the structures. Also, it has proven efficient for computing the structure responses much more quickly than a full FE analysis (about $90 - 95\%$ time saving, even more). This appears to be crucial, e.g., to perform Monte Carlo simulations where the sensitivity of the structure responses to random parameters, eventually together with random mesh distortions (geometric variability), could be of concern.

References

[1] J.-M. Mencik, Model reduction based on matrix interpolation and distorted finite element meshes for dynamic analysis of 2d nearly periodic structures, Finite Elements in Analysis and Design 188 (2021) 103518. doi:10.1016/j.finel.2021.103518.

[2] B. Besselink, U. Tabak, A. Lutowska, N. van de Wouw, H. Nijmeijer, D. Rixen, M. Hochstenbach, W. Schilders, A comparison of model reduction techniques from structural dynamics, numerical mathematics and systems and control, Journal of Sound and Vibration 332 (2013) 4403–4422. doi:10.1016/j.jsv.2013.03.025.

[3] Z. Bai, Krylov subspace techniques for reduced-order modeling of large-scale dynamical systems, Applied Numerical Mathematics 43 (1-2) (2002) 9–44. doi:10.1016/S0168-9274(02)00116-2.

[4] A. C. Antoulas, D. C. Sorensen, Approximation of large-scale dynamical systems: An overview, Technical Report, Electrical and Computer Engineering, Rice University, Houston, TX, 2001.

[5] R. Guyan, Reduction of stiffness and mass matrices, AIAA Journal 3 (2) (1965) 380. doi:10.2514/3.2874.

[6] L. Suarez, M. Singh, Dynamic condensation method for structural eigenvalue analysis, AIAA Journal 30 (4) (1992) 1046–1054. doi:10.2514/3.11026.

[7] N. Bouhaddi, R. Fillod, Substructuring using a linearized dynamic condensation method, Computers and Structures 45 (4) (1992) 679–683. doi:10.1016/0045-7949(92)90486-J.

[8] M. Friswell, S. Garvey, J. Penny, Model reduction using dynamic and iterated irs techniques, Journal of Sound and Vibration 186 (2) (1995) 311–323. doi:10.1006/jsvi.1995.0451.

[9] Y. Xia, R. Lin, Improvement on the iterated irs method for structural eigensolutions, Journal of Sound and Vibration 270 (4-5) (2004) 713–727. doi:10.1016/S0022-460X(03)00188-3.

[10] D. Choi, H. Kim, M. Cho, Iterative method for dynamic condensation combined with substructuring scheme, Journal of Sound and Vibration 317 (1-2) (2008) 199–218. doi:10.1016/j.jsv.2008.02.046.

[11] J.-H. Kim, S.-H. Boo, P.-S. Lee, A dynamic condensation method with free interface substructuring, Mechanical Systems and Signal Processing 129 (2019) 218–234. doi:10.1016/j.ymssp.2019.04.021.

[12] S. Weng, A.-Z. Zhu, H.-P. Zhu, Y. Xia, L. Mao, P.-H. Li, Dynamic condensation approach to the calculation of eigensensitivity, Computers and Structures 132 (2014) 55–64. doi:10.1016/j.compstruc.2013.10.012.

[13] S. Weng, W. Tian, H. Zhu, Y. Xia, F. Gao, Y. Zhang, J. Li, Dynamic condensation approach to calculation of structural responses and response sensitivities, Mechanical Systems and Signal Processing 88 (2017) 302–317. doi:10.1016/j.ymssp.2016.11.025.

[14] L. Rouleau, J.-F. Deü, A. Legay, A comparison of model reduction techniques based on modal projection for structures with frequency-dependent damping, Mechanical Systems and Signal Processing 90 (2017) 110–125. doi:10.1016/j.ymssp.2016.12.013.

[15] A. Cunha-Filho, Y. Briend, A. de Lima, M. Donadon, An efficient iterative model reduction method for aeroviscoelastic panel flutter analysis in the supersonic regime, Mechanical Systems and Signal Processing 104 (2018) 575–588. doi:10.1016/j.ymssp.2017.11.018.

[16] A. Lima, N. Bouhaddi, D. Rade, M. Belonsi, A time-domain finite element model reduction method for viscoelastic linear and nonlinear systems, Latin American Journal of Solids and Structures 12 (6) (2015) 1182–1201. doi:0.1590/1679-78251695.

[17] Z. Ding, L. Li, J. Kong, L. Qin, A modal projection-based reduction method for transient dynamic responses of viscoelastic systems with multiple damping models, Computers and Structures 194 (2018) 60–73. doi:10.1016/j.compstruc.2017.09.004.

[18] D. de Klerk, D. Rixen, S. Voormeeren, General framework for dynamic substructuring: history, review, and classfication of techniques, AIAA Journal 46 (5) (2008) 1169–1181. doi:10.2514/1.33274.

[19] R. Craig, M. Bampton, Coupling of substructures for dynamic analyses, AIAA Journal 6 (7) (1968) 1313–1319. doi:10.2514/3.4741.

[20] R. MacNeal, A hybrid method of component mode synthesis, Computers and Structures 1 (4) (1971) 581–601. doi:10.1016/0045-7949(71)90031-9.

[21] N. Bouhaddi, J. Lombard, Improved free-interface substructures representation method, Computers and Structures 77 (3) (2000) 269–283. doi:10.1016/S0045-7949(99)00219-9.

[22] D. Rixen, A dual craig-bampton method for dynamic substructuring, Journal of Computational and Applied Mathematics 168 (1-2) (2004) 383–391. doi:10.1016/j.cam.2003.12.014.

[23] F. Gruber, D. Rixen, Evaluation of substructure reduction techniques with fixed and free interfaces, Journal of Mechanical Engineering 62 (7-8) (2016) 452–462. doi:10.5545/sv-jme.2016.3735.

[24] S. Voormeeren, D. Rixen, A family of substructure decoupling techniques based on a dual assembly approach, Mechanical Systems and Signal Processing 27 (2012) 379–396. doi:10.1016/j.ymssp.2011.07.028.

[25] D. Klerk, D. J. Rixen, J. de Jong, The frequency based substructuring (fbs) method reformulated according to the dual domain decomposition method, Proceedings of the 24th International Modal Analysis Conference (IMAC), St. Louis, USA (136) (2006) 1–14.

[26] J.-G. Kim, P.-S. Lee, An enhanced craig-bampton method, International Journal For Numerical Methods in Engineering 103 (2015) 79–93. doi:10.1002/nme.4880.

[27] J.-H. Kim, J. Kim, P.-S. Lee, Improving the accuracy of the dual craig-bampton method, Computers and Structures 191 (2017) 22–32. doi:10.1016/j.compstruc.2017.05.010.

[28] J. Qiu, Z. Ying, F. Williams, Exact modal synthesis techniques using residual constraint modes, International Journal for Numerical Methods in Engineering 40 (13) (1997) 2475–2492. doi:10.1002/(SICI)1097-0207(19970715)40:13<2475::AID-NME176>3.0.CO;2-L.

[29] M. Géradin, D. Rixen, A 'nodeless' dual superelement formulation for structural and multibody dynamics application to reduction of contact problems, International Journal for Numerical Methods in Engineering 106 (10) (2016) 773–798. doi:10.1002/nme.5136.

[30] J. Kim, S. Boo, P. Lee, An enhanced amls method and its performance, Computer Methods in Applied Mechanics and Engineering 287 (2015) 90–111. doi:10.1016/j.cma.2015.01.004.

[31] U. Kirsch, Implementation of combined approximations in structural optimization, Computers and Structures 78 (1-3) (2000) 449–457. doi:10.1016/S0045-7949(00)00093-6.

[32] S. Balmès, Optimal ritz vectors for component mode synthesis using the singular value decomposition, AIAA Journal 34 (1996) 1256–1260. doi:10.2514/3.13221.

[33] G. Masson, B. A. Brik, S. Cogan, N. Bouhaddi, Component mode synthesis (cms) based on an enriched ritz approach for efficient structural optimization, Journal of Sound and Vibration 296 (2006) 845–860. doi:10.1016/j.jsv.2006.03.024.

[34] A. Bouazzouni, G. Lallement, S. Cogan, Selecting a ritz basis for the reanalysis of the frequency response functions of modified structures, Journal of Sound and Vibration 199 (2) (1997) 309–322. doi:10.1006/jsvi.1996.0617.

[35] M. Guedri, A. de Lima, N. Bouhaddi, D. Rade, Robust design of viscoelastic structures based on stochastic finite element models, Mechanical Systems and Signal Processing 24 (1) (2010) 59–77. doi:10.1016/j.ymssp.2009.03.010.

[36] V. Silva, A. de Lima, N. Bouhaddi, H. Lacerda, Uncertainty propagation and experimental verification of nonlinear viscoelastic sandwich beams, Mechanical Systems and Signal Processing 132 (2019) 654–669. doi:10.1016/j.ymssp.2019.07.022.

[37] U. Kirsch, A unified reanalysis approach for structural analysis, design, and optimization, Structural and Multidisciplinary Optimization 25 (2003) 67–85. doi:10.1007/s00158-002-0269-0.

[38] C. Soize, Reduced models in the medium frequency range for general dissipative structural-dynamics systems, European Journal of Mechanics - A/Solids 17 (4) (1998) 657–685. doi:10.1016/S0997-7538(99)80027-8.

[39] B. V. den Nieuwenhof, J.-P. Coyette, Modal approaches for the stochastic finite element analysis of structures with material and geometric uncertainties, Computer Methods in Applied Mechanics and Engineering 192 (33-34) (2003) 3705–3729. doi:10.1016/S0045-7825(03)00371-2.

[40] M. Guedri, N. Bouhaddi, R. Majed, Reduction of the stochastic finite element models using a robust dynamic condensation method, Journal of Sound and Vibration 297 (1-2) (2006) 123–145. doi:10.1016/j.jsv.2006.03.046.

[41] A. Batou, C. Soize, Stochastic reduced-order model in low-frequency dynamics in presence of numerous local elastic modes, Proceedings of RASD 2010 - 10th International Conference on Recent Advances in Structural Dynamics, Southampton, UK, 12-14 July.

[42] A. Batou, A global/local probabilistic approach for reduced-order modeling adapted to the low- and mid-frequency structural dynamics, Computer Methods in Applied Mechanics and Engineering 294 (2015) 123–140. doi:10.1016/j.cma.2015.06.007.

[43] H. Panzer, J. Mohring, R. Eid, B. Lohmann, Parametric model order reduction by matrix interpolation, at-Automatisierungstechnik 58 (8) (2010) 475–484. doi:10.1524/auto.2010.0863.

[44] S. Balmès, Parametric families of reduced finite element models theory and applications, Mechanical Systems and Signal Processing 10 (4) (1996) 381–394. doi:10.1006/mssp.1996.0027.

[45] T. Chan, G. Golub, R. J. Leveque, Algorithms for computing the sample variance: analysis and recommendations, The American Statistician 37 (3) (1983) 242–247. doi:10.1080/00031305.1983.10483115.

[46] E. Hinton, B. Bicanic, A comparison of Lagrangian and Serendipity Mindlin plate elements for free vibration analysis, Computers and Structures 10 (1979) 483–493. doi:10.1016/0045-7949(79)90023-3.